Investigation of the $^{14}C + \alpha$ molecular configuration in ^{18}O by means of transfer and sequential decay reaction

B. Yang,[1] Y. L. Ye,[1,*] J. Feng,[1] C. J. Lin,[2] H. M. Jia,[2] Z. H. Li,[1] J. L. Lou,[1] Q. T. Li,[1] Y. C. Ge,[1] X. F. Yang,[1] H. Hua,[1] J. Li,[3] H. L. Zang,[1] Q. Liu,[1] W. Jiang,[4] C. G. Li,[1] Y. Liu,[1] Z. Q. Chen,[1] H. Y. Wu,[1] C. G. Wang,[1] W. Liu,[1] X. Wang,[1] J. J. Li,[1] D. W. Luo,[1] Y. Jiang,[1] S. W. Bai,[1] J. Y. Xu,[1] N. R. Ma,[2] L. J. Sun,[2] D. X. Wang,[2] Z. H. Yang,[5,6] and J. Chen[3]

[1] *School of Physics and State Key Laboratory of Nuclear Physics and Technology, Peking University, Beijing 100871, China*
[2] *China Institute of Atomic Energy, Beijing 102413, China*
[3] *Physics Division, Argonne National Laboratory, Argonne, Illinois 60439, USA*
[4] *Institute of High Energy Physics, CAS, Beijing 100049, China*
[5] *Research Center for Nuclear Physics, Osaka University, 10-1 Mihogaoka, Ibaraki 567-0047,Japan*
[6] *RIKEN Nishina Center, 2-1 Hirosawa, Wako, Saitama 351-0198, Japan*

(Dated: Received day month year; published day month year)

A multinucleon transfer and cluster-decay experiment, namely ^{9}Be(^{13}C,^{18}O* $\rightarrow^{14}$C + α)α, was performed at a beam energy of 65 MeV. Resonant states in ^{18}O from 7 to 19 MeV, including some newly observed ones, are reconstructed with high resolution, based on the coincident detection of various combinations of the final fragments. The α-decay branching ratios for 14 states are extracted from both the invariant-mass and missing-mass measurements. Angular correlation analysis was conducted for the 10.3-MeV (4^{+}) state. The present work supports the existence of the positive-parity rotational band associated with the $^{14}C + \alpha$ molecular structure in ^{18}O, but the negative-parity band members were not identified.

I. INTRODUCTION

The concept of nucleon clustering has been adopted to explain some peculiar structure phenomena in light nuclei [1–3]. In the case of α-conjugate $N = Z$ nuclei, cluster structure tends to be formed at around the cluster-separation threshold, as depicted by the famous Ikeda diagram [4]. For nuclei away from the β-stability line, the extra neutron may help to stabilize the nuclear-molecular system, leading to much more abundant cluster configurations [1]. Investigations on neutron-excess beryllium isotopes have revealed such kind of molecular structure built on 2-α cores [5–12]. For neutron-rich carbon isotopes, typical 3-α-core systems, the π-bond or σ-bond linear-chain and triangle molecular structures have been theoretically proposed and experimentally evidenced [13–17]. When further extending to oxygen isotopes, such as ^{18}O, some mass asymmetric cluster structures, e.g., $^{14}C + \alpha$, are expected to be formed, which are characterized by the intrinsic reflection asymmetry [18–20].

According to the cluster (molecular) description of the nuclear system, the broken reflection symmetry may give rise to the splitting of the rotational bands into parity inversion doublets (Ref. [20] and references therein). Indeed these doublet partner bands, with a splitting of a few MeV, have been well established for $N = Z$ even-even light nuclei, such as ^{16}O and ^{20}Ne, based on extensive experimental and theoretical studies [20–23]. Much effort has also been made to search for the members of the parity-inversion doublet bands in neutron rich nuclei, to understand the role of the valence neutrons [18–20, 24]. ^{18}O has been an interesting candidate of these studies owing to the interplay between its typical $^{16}O + 2n$ single-particle structure and $^{x}C + \alpha + (14 - x)n$ cluster configurations [19, 24]. It is worth noting that the ^{14}C nucleus is a well-binding core candidate, quite similar to ^{12}C or ^{16}O [20]. So far the inclusive excitation-energy spectra for ^{18}O have been measured by many experiments and are summarized in Refs. [20, 25], whereas the measurement directly related to cluster contents inside the nucleus is still very limited. For states above the cluster-separation energy, the latter has normally relied on the coincident detection of the sequential cluster-decay fragments, following the excitation induced by inelastic scattering or transfer reaction. The cluster-decay measurement has several advantages. First, it is sensitive only to the states with significant cluster contents and may therefore, to a large extent, avoid the very high level density at the high-excitation-energy region where the cluster structures of interest often reside [26]. Second, it may provide an independent way to determine the spin of the reconstructed resonant state through the sensitive angular correlation method [26, 27]. This method is particularly useful at high excitation energy where the usual differential cross-section analysis faces large uncertainties. Third, the cluster-decay branching ratio (BR) is directly related to the cluster spectroscopic factor (SF) of the resonance, which is a quantitative measure of the cluster formation probability in the state [6, 10]. There have been a few experiments that have measured coincidentally the decay fragments from ^{18}O resonances [26, 28–30], but mostly they suffered from small-correlation-angle coverage and from lack of BR measurement. The latter requires the

* Corresponding author: yeyl@pku.edu.cn

detection of both decay fragments and recoil fragments. We note that the resonant scattering experiments using thick targets provide also rich information on certain cluster configurations [24], but their inclusive nature and numerous input parameters might lead to some inconsistent results [15], which need to be compared, when possible, with exclusive coincident measurements (see Sec. IV for more discussion). Therefore it would be essential to apply more advanced detector systems to expand the cluster-decay correlation measurement.

Using basically the inclusive data with information on excitation energies and cross sections, von Oertzen *et al* [20] tried to place various ^{18}O states into the predicted molecular rotational bands, including the ones built on $K^\pi = 0_1^+$ and $K^\pi = 1^-$ (with the single-particle configuration), on $K^\pi = 0_2^\pm$ (partner bands with the $^{14}\mathrm{C} \otimes \alpha$ structure), and on $K^\pi = 0_4^\pm$ (partner bands with the $^{12}\mathrm{C} \otimes 2\mathrm{n} \otimes \alpha$ structures). Of course, these tentative classifications need to be justified by experiments. Very recently, a resonant scattering experiment using a radioactive ^{14}C beam and a thick He-gas target, together with R-matrix analysis, has resulted in quite a different conclusion about clustering in ^{18}O [24]. Particularly, the members of the negative-parity rotational band were not confirmed. The authors of Ref. [24] emphasized the importance of measuring the spins and cluster-decay BRs.

In an attempt to further understanding of the parity-inversion partner doublets in ^{18}O, we conducted a multinucleon transfer and sequential cluster-decay experiment, namely ^{9}Be(^{13}C,^{18}O$^* \rightarrow ^{14}$C + $\alpha)\alpha$, with a beam energy of 65 MeV. Coincident detection was realized for various combinations of the final fragments. High-resolution excitation-energy spectra were obtained, partially with information on cluster BRs and SFs.

II. EXPERIMENTAL DETAILS

The experiment was carried out at the HI-13 tandem accelerator facility at the China Institute of Atomic Energy in Beijing [14]. A 65-MeV ^{13}C beam with an intensity of approximately 2.5 enA was incident on a 259 μg cm^{-2} self-supporting ^{9}Be target. The multinucleon transfer reaction ^{9}Be(^{13}C,^{18}O$^*)\alpha$ was used to populate states in ^{18}O. The recoil α particle and the two decay fragments $^{14}\mathrm{C} + \alpha$ were detected by an array of six charged-particle telescopes, namely L0, R0, L1, R1, L2, and R2, which were symmetrically placed on both sides of the beam axis as schematically displayed in Fig. 1.

Two forward telescopes (L0 and R0) were centered at 24° with respect to the beam direction and were placed at a distance of about 160 mm from the target center. Each of them consists of two layers of double-sided silicon strip detectors (DSSDs), with thicknesses of about 40 μm (W1) and 300 μm (BB7), and one large-size silicon detector (SSD), with a thickness of 1500 μm (MSX40).

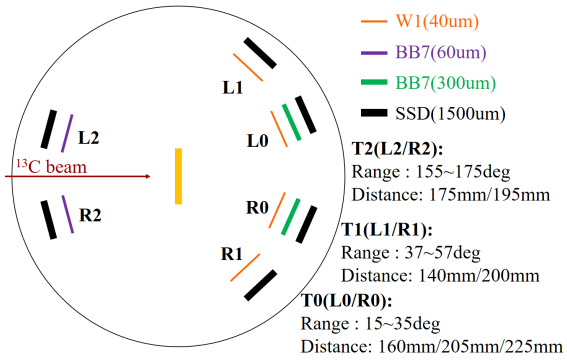

FIG. 1. Schematic view of the experimental setup.

The active areas are 50 mm × 50 mm for W1 and 64 mm × 64 mm for BB7 and MSX40. For DSSDs the front and back sides were segmented into 16 (for W1) or 32 (for BB7) strips, providing good two-dimensional position resolutions and the ability to record multihit events in one telescope. Other two telescopes (L1 and R1), each composed of one DSSD (W1, 40 μm) and one SSD (MSX40, 1500 μm), were centered at 47°. The backward telescopes (L2 and R2), each composed of one DSSD (BB7, ∼60 μm) and one SSD (MSX40, 1500 μm), were centered at 165° to detect the recoil light particles.

The applied transfer-decay reaction ^{9}Be(^{13}C, ^{18}O$^* \rightarrow ^{14}$C + $\alpha)\alpha$ possesses a quite large reaction energy (Q value) of 6.603 MeV. This is helpful for the population of high-lying states in the final nucleus and also for the selection of the reaction channel of interest, as demonstrated in our previous work [14]. The only contamination channel comes from the reaction ^{9}Be(^{13}C,^{8}Be$\rightarrow$ α + $\alpha)^{14}$C, which has the same final mass combination and thus the same Q value. In this channel, two α-particles are produced from the ^{8}Be decay after one-neutron transfer from ^{9}Be to ^{13}C. In principle this contamination channel can be separated based on its very different kinematics behavior and by using the Dalitz plot [16].

Two α-particles from the targeted reaction ^{9}Be(^{13}C, ^{18}O$^* \rightarrow ^{14}$C + $\alpha)\alpha$, namely the decay one and the recoil one, can also be discriminated according to the kinematics, subject to a limit on the excitation energy. Figure 2 shows the Monte Carlo simulation of the kinematics, assuming 18-MeV excitation in ^{18}O. In the plot, the black solid line represents the recoil α particle, whereas the color-covered area stands for the decay α particle from the excited ^{18}O. The black solid line tends to approach the color band with increasing excitation energy in ^{18}O. The critical energy is at about 19 MeV, below which the recoil α particle can be clearly distinguished. In the present work we focus on the resonances below 19 MeV, and therefore the source of the α particles can be uniquely determined.

Once two out of three final-state particles are identified by the energy loss versus remaining energy (ΔE-E)

method using the telescope, the kinematics quantities of the third particle can be deduced according to the energy and momentum conservation [31]. Hence the resonant states in ^{18}O can be reconstructed based on various combinations of detected particles [8, 9, 14]. For instance, states at low relative energies could be deduced from events with both ^{14}C and decay α particles being detected in the same telescope (most likely the forward L0 or R0). For events with two detected α particles, the best energy resolution can be obtained for resonances reconstructed from the deduced ^{14}C plus the detected decay α particle (see next section). In particular when using α particles detected by the backward telescope L2/R2 in coincidence with α particles detected at forward angles, the corresponding ^{18}O* should emit at very small center-of-mass (c.m.) angles. These events can be used to extract the spin of the ^{18}O* state, as demonstrated in Sec. III(C) for the 10.3-MeV resonance.

III. EXPERIMENTAL RESULTS

A. Observed excitation energy spectra

The reaction Q value is defined by the mass deficit between the initial and final particles and therefore is useful to determine the reaction channels. It can be calculated from the energy released from the following reaction:

$$Q = E_{\rm tot} - E_{\rm beam} = \sum E_i - E_{\rm beam}, \qquad (1)$$

where $E_{\rm beam}$ and E_i are the incident beam energy and the energies for the final particles, respectively. Figure 3 shows the experimental Q-value spectra for events with detected ^{14}C + α (the blue dotted line) and detected α + α (the black solid line). In both cases, a distinct peak stands at ~6.6 MeV, corresponding to all three final particles on their ground states ($Q_{\rm ggg}$ peak). In the following analysis of the resonances, we always apply a gate on the $Q_{\rm ggg}$ peak to constrain the reaction channel. The difference in $Q_{\rm ggg}$ peak widths is essentially due to the different energy resolutions between ^{14}C and α detections. This difference is also exhibited in the reconstructed excitation-energy spectra of ^{18}O as demonstrated in Fig. 4, indicating the remarkable advantage of using the detected 2-α events. We notice that the latter approach was not conducted in previous experiments [26, 28, 29, 32].

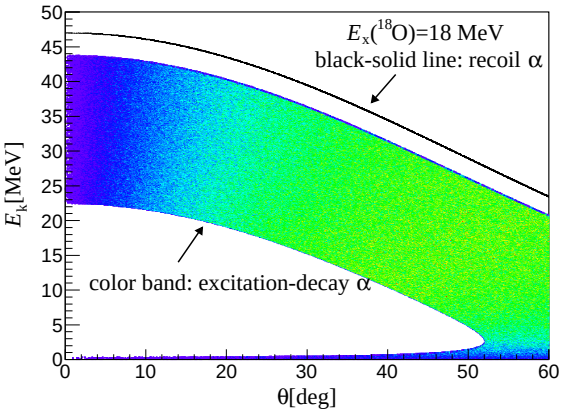

FIG. 2. Relationship between energy and angle (Lab) for the recoil α particles (the black solid line) and for the decay α particles originated from excited ^{18}O (18 MeV) (the color band).

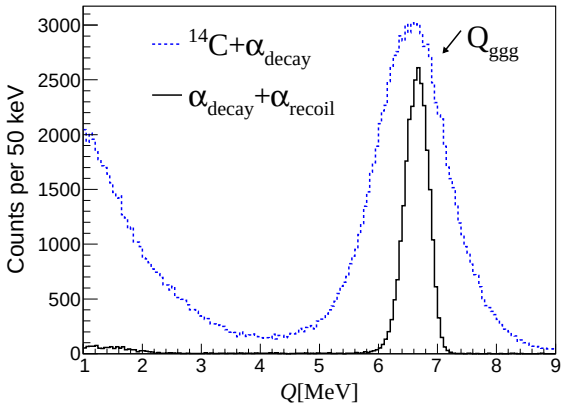

FIG. 3. Q-value spectra obtained from the present measurement, for events with detected ^{14}C + α (the dotted line) or α + α (the solid line) fragments.

In Fig. 5(a), we summarize the resonant states observed in the present experiment based on the ^{18}O$^* \rightarrow ^{14}$ C + α detection and reconstruction. The observed excitation-energy ranges from the α-decay threshold at 6.23 MeV up to about 19 MeV. States below 10 MeV are reconstructed from events with detected ^{14}C + α fragments in the same telescope (L0 or R0) while those from 10 to 19 MeV are reconstructed from events with detected two-α fragments from L0 + R0 telescopes. This choice is based on the angular acceptance of the telescopes for the corresponding events. For comparison, we also plot the spectra from two previous similar measurements in Fig. 5(b) [28] and Fig. 5(c) [26]. We can see that most states observed in the present work agree very well with the previously reported ones, indicating the reliability of the present measurement. Owing to the significantly higher energy resolution as well as the broader excitation-energy coverage, new information is obtained from the present measurement. First, three states at 11.1, 11.5, and 11.7 MeV are well resolved now in Fig. 5(a) , whereas they are overlapped in Fig. 5(b) [28] and Fig. 5(c) [26] and in other α-decay observations [29, 32]. In addition, a series of distinct resonances above 12 MeV are clearly observed, with much better visibility as compared to previously reported spectra. Particularly, several α-decay states above 15 MeV are clearly observed for the first time. All identified resonant states are listed in Table I.

B. Branching Ratio

To increase the reconstruction efficiency, the trigger algorithm of the detection system relied mainly on the two fold coincident signals. In the meantime, events having a single hit were also recorded at the 1/100 sampling rate to keep the inclusive results. Therefore, based on the detected recoil α particles ($\alpha_{\rm recoil}$), both the missing-mass (MM) (inclusive) spectrum [33] and the invariant-mass (IM) spectrum (from detected $\alpha_{\rm recoil}$ + $\alpha_{\rm decay}$ and deduced ^{14}C) [14] can be obtained for the excitation-energy range above 10 MeV [Fig. 5(a)]. In Fig. 6, the excitation-energy spectrum of ^{18}O deduced by the MM method is plotted and compared to the IM spectrum.

Detailed Monte Carlo simulations have been performed to estimate the detection efficiencies for both missing-mass and invariant-mass measurements. The real detector geometries and properties, the beam spot size and the target thickness, were considered in the simulation. The angular distribution of the reaction is assumed to be isotropic because the geometrical coverage of the detection system is quite similar in the c.m. system for both MM or IM measurements and only the relative efficiency matters in the following branching ratio (BR) deduction [34].

The BR is defined as

$$BR = \frac{N_{\rm IM}/\epsilon_{\rm IM}}{100\times N_{\rm MM}/\epsilon_{\rm MM}}, \qquad (2)$$

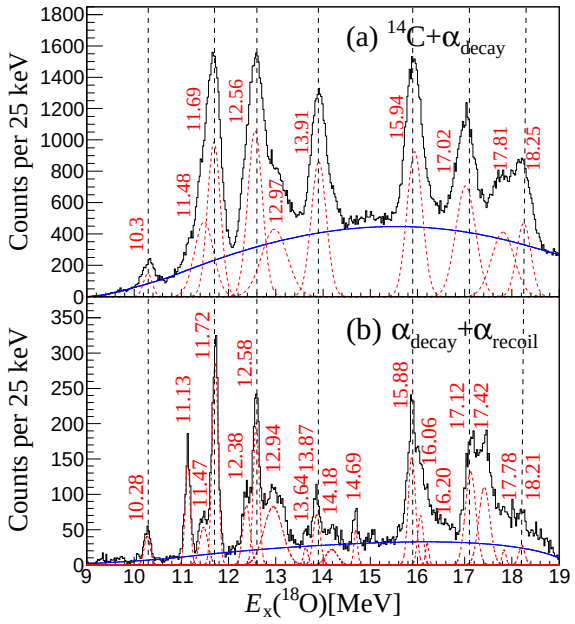

FIG. 4. ^{18}O* excitation-energy spectra from (a) events with detected ^{14}C + α and (b) events with detected α + α. Peaks in each spectrum are fitted by a number of Gaussian functions (red dotted lines) plus a continuous background (the blue smooth line).

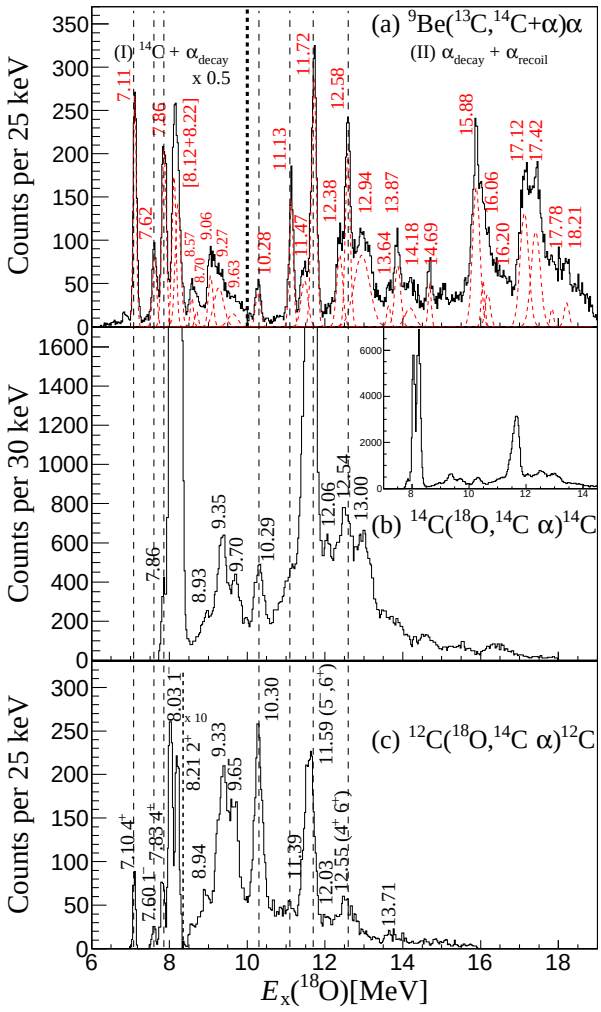

FIG. 5. (a) Excitation-energy spectrum of ^{18}O obtained from the present experiment. States below 10 MeV are reconstructed from events with detected ^{14}C + α fragments from the same telescope (L0 or R0), while states between 10 and 19 MeV are from events with detected two-α (and deduced ^{14}C) fragments from L0 + R0 telescopes. These resonances are compared with the previous results: (b) from Ref. [28] and (c) from Ref. [26].

where $N_{\rm IM}$ ($N_{\rm MM}$) denotes the number of events extracted from a resonance peak (Fig. 6) and $\epsilon_{\rm IM}$ ($\epsilon_{\rm MM}$) is the corresponding efficiency determined from the simulation. The factor 100 is used to account for the sampling rate for the MM measurement. The obtained results are listed in Table I. $E_{\rm x}$ from the MM method is omitted in the table because it is less accurate and very close to that from the IM method. In Table I only the statistical errors are presented for the BRs. In addition a systematical error of about 30% is estimated, which comes basically from the background estimation for the MM spectrum. We note that the BRs could only be extracted for part of the observed resonances (from 10 to 17 MeV) due to the requirement of both the $\alpha_{\rm recoil}$ detection and the $\alpha_{\rm decay}$ detection and the significance of

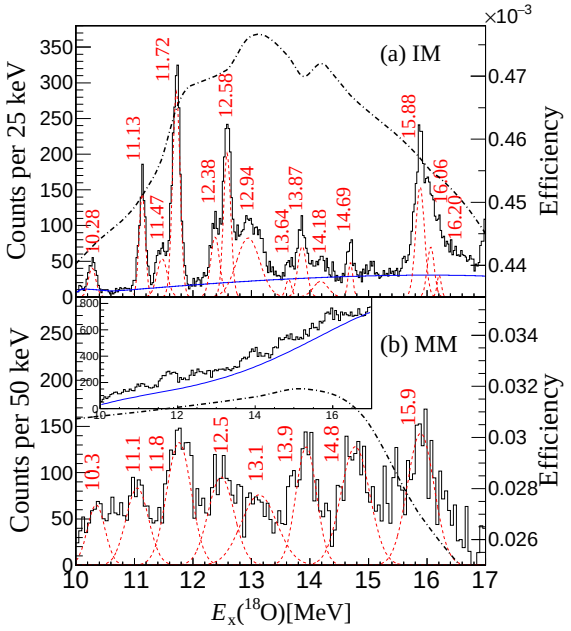

FIG. 6. (a) The invariant-mass spectrum reconstructed from $^{18}O^* \rightarrow ^{14}C + \alpha$ decay [using events with detected 2-α (by L0 + R0) and deduced ^{14}C], in comparison to (b) the corresponding missing-mass spectrum using events with detected recoil α particles. Each spectrum is fitted by a number of Gaussian-function peaks (red dashed lines) plus a smooth background (the blue solid line). For a better view of the peak, the structure built on the large background as exhibited in the inset of panel (b), the inclusive missing-mass spectrum is plotted with the background subtracted. In both cases, the black dot-dashed lines show the simulated experimental detection efficiency.

the resonance peak in the MM spectrum. Also due to the worse energy resolution of the MM spectrum, in which one peak may cover several peaks of the IM spectrum, the associated BRs appear as the lower limits in Table I.

For each resonant peak in Fig. 6(a), the measured peak width can be fitted by the convolution of the physical resonance function (Breit-Wigner form) with the detection resolution function (Gaussian form). Monte Carlo simulation was conducted to estimate the detection resolution, which includes some parameters such as the detector performances, the beam properties, and the system alignment. The simulated energy-resolution curve can be calibrated by using some known resonances. Based on the inclusive measurement by using the Q3D magnetic spectrograph, precise results for the total widths (TWs) of some resonances in ^{18}O were reported in Ref. [20]. In particular, the narrow resonances at 11.12, 12.57, and 14.64 MeV appear distinctly in both Ref. [20] and in present Fig. 6(a). The reported physical TWs of these three states [20] were used to fix the calibrated detection resolution, which ranges from 125 keV at 10 MeV to 141 keV at 16 MeV. Finally the TW of each identified resonance in Fig. 6(a) is extracted and listed in Table I, together with the statistical error. In addition, another systematic uncertainty of about 10% is expected, due basically to the determination of the energy resolution of the detection system. The presently obtained TWs are quite similar to those reported in Ref. [24] (also listed in Table I for comparison), when there appear clear resonant peaks in both measurements. However, significant difference happens for states at 13.64, 14.18, and 14.69 MeV. We note that the presently obtained smaller TW values are based on the clearly observed resonant peaks from the exclusive cluster-decay measurement, whereas the results of Ref. [24] for these states comes from fittings to the inclusive spectra having broad and smooth shapes around these energies.

The dimensionless reduced α-width θ_α^2 (cluster SF) is also deduced and listed in Table I, in comparison to the results of Ref. [24]. The definition and the channel radius (5.2 fm) used in the deduction are exactly the same as those in Ref. [24]. These results are discussed in more detail in Sec. IV.

C. Spin analysis of the 10.3 MeV state

Angular correlation between the decay fragments is a sensitive tool to determine the spin of the mother nucleus [27]. The two angles involved here are θ^*, the center-of-mass scattering angle of the mother nucleus on its resonant state, and ψ, the angle between the relative velocity vector of the two decay fragments and the beam axis [27]. When the resonant nucleus is emitted to angles around $\theta^* = 0^\circ$ and decays into spin-0 final fragments, the correlation function is simplified into a shape proportional to the square of the Legendre polynomial of order J, namely $|P_J(\cos(\psi))|^2$, with J being the spin of the mother nucleus [35]. For the detection away from $\theta^* = 0^\circ$, the structure of the correlation function shifts according to $\psi' = \psi - \frac{l_i - J}{J}\theta^*$, where l_i is the dominant partial wave in the entrance channel [27, 28, 35]. The values of l_i can be evaluated via $l_i = r_0(A_p^{1/3} + A_t^{1/3})\sqrt{2\mu E_{c.m.}}$[28], where A_p and A_t are mass numbers of the beam and the target particles, respectively; μ is the reduced mass; and $E_{c.m.}$ the center-of-mass energy. In the present work, we take $r_0 = 1.2$ fm, which leads to $l_i = 13.9\ \hbar$.

In the present measurement, some resonances in ^{18}O can be reconstructed from events with detected 2-α particles, namely the decay one from the forward L0/R0 telescope and the recoil one from the backward L2/R2 telescope, respectively. In this case, the reconstructed ^{18}O, emitting mostly to very forward c.m. angles, is suitable for the angular correlation analysis. The resonances for $\theta^* < 10^\circ$ are plotted in Fig. 7(a). Because the recoil α-particles at backward angles may be contaminated by the above mentioned $^9Be(^{13}C,^8Be\rightarrow \alpha + \alpha)^{14}C$ background channel, we have conducted the Dalitz-type analysis as shown in Fig. 7(b). Indeed a horizontal line appears at around 16.9 MeV in ^8Be excitation, resulting in a higher continuous background

in the excitation-energy spectrum of ^{18}O from 7 to 12 MeV.

The state at 10.3 MeV is a good candidate for angular correlation analysis, owing to its clear peak identification and relatively large ψ-angle coverage. The yield under this peak is extracted in each bin of $\Delta\cos(\psi')$=0.05. Because the squared Legendre polynomials are even functions, i.e., $|P_J(\cos(\psi'))|^2 = |P_J(|\cos(\psi')|)|^2$, we present the $|\cos(\psi')|$ distribution instead of $\cos(\psi')$. In Fig. 8, a uniformly distributed background is assumed for the uncorrelated component. After the correction on detection efficiency, a theoretical function composed of a Legendre polynomial plus a constant background is used to evaluate the angular correlation. As shown in Fig. 8, the spin-parity assignment of 4^+ gives rise to an excellent fit to the data. Any other spin number would give a much worse description with a much larger $\bar{\chi}^2$ value.

The states above 11 MeV show quite weak structure in their angular correlation due to the partial overlap of the nearby peaks or the large variation of the detection efficiency curve. For these states more work is still needed to determine their spins.

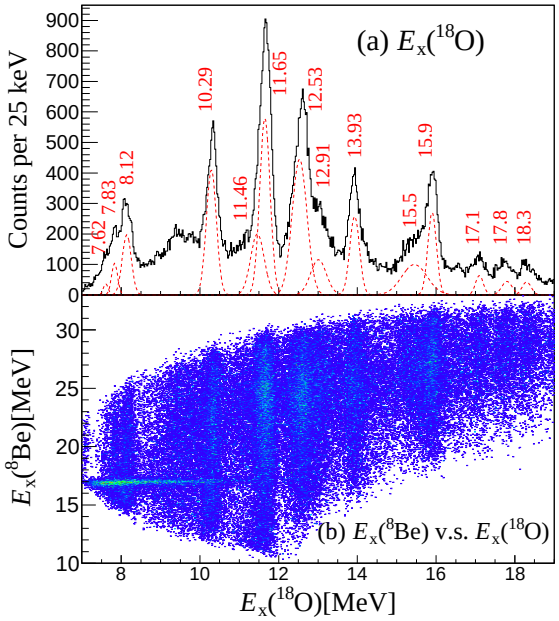

FIG. 7. (a) Excitation-energy spectrum for ^{18}O, reconstructed from events with one α-particle detected by the L0/R0 telescope while another is detected by the R2/L2 telescope. (b) Dalitz-type two-dimensional excitation-energy spectrum for reconstructed ^{8}Be (from 2-α) versus ^{18}O (from $\alpha + ^{14}$C$_{\rm deduced}$).

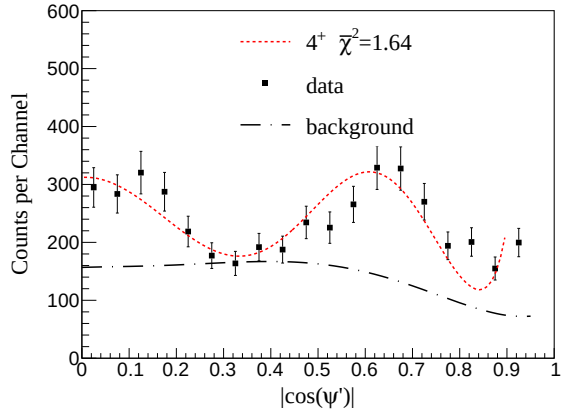

FIG. 8. The angular correlation for the 10.3-MeV state, compared with the Legendre polynomials of order 4 (the red dotted line). A uniformly distributed background is assumed for the uncorrelated component (the long dot-dashed line). All the theoretical angular distributions are corrected for the detection efficiency. The corresponding reduced $\bar{\chi}^2$ is also indicated in this plot.

IV. DISCUSSION

For decades, numerous attempts, both in theory [18, 19] and experiment [20, 24, 26, 28, 36], have been devoted to seeking for members of the inversion doublet rotational bands with intrinsic molecular structure in ^{18}O. However the assignment of the experimentally observed states into such band members remains controversial, due basically to the difficulties in determining the spins and the cluster-decay BRs [24]. Using the presently obtained TWs and BRs for 14 states between 10 and 16.5 MeV in ^{18}O, together with possible spin assignments suggested from the literature, we are able to deduce the SFs for the corresponding states [6, 10]. The results are also listed in Table I. These data are very useful for further understanding the parity-inversion doublet states in ^{18}O.

A. Discussion on the positive-parity band

The positive-parity rotational band of the ^{14}C + α cluster structure in ^{18}O has been suggested in several theoretical [18, 19] and experimental [20, 28–30] work. The first four members of this band are consistently associated with the observed states: 0^+ (3.63 MeV), 2^+ (5.24 MeV), 4^+ (7.11 MeV), and 6^+ (11.69 MeV), respectively. The first two members can not be observed from the α-decaying experiment because they are below the cluster-separation threshold. The 7.11-MeV state has been observed, repeatedly from the α-decay channel, as a narrow and strong peak (Fig. 5 and Table I). Its spin-parity is well determined as 4^+.

In Ref. [18], the 6^+ state was predicted at 11.6 MeV with a dimensionless reduced α-width (namely the cluster SF) of 0.15. This is consistent with a strong cluster state at 11.7 MeV (6^+), determined by Avila *et al.* [24] through R-matrix analysis. However, in the previous breakup experiments [26, 28], a strong resonance was observed at around 11.6 MeV, with a spin-parity assignment of 5^-, based on the angular correlation analysis. This contradiction may be explained

TABLE I. Summary of the excited states with $\alpha + {}^{14}$C configuration, observed in the present ^{9}Be(^{13}C,^{18}O* $\rightarrow{}^{14}$C+α)α reaction. For comparison, results from previous resonant scattering and cluster-decay measurements are also presented. Spins in brackets mean tentative assignments. For comparative purposes, the dimensionless reduced α width θ_α^2 (cluster SF) is deduced under the same definition as in Ref. [24], namely $\theta_\alpha^2 = \gamma^2/(\hbar^2/\mu R^2)$ and R =5.2 fm. In this table, only statistical errors are presented for all TWs and BRs extracted in the present work.

Present work					Resonant scattering [24]					^{14}C(^{18}O,^{14}Cα)^{14}C [28]		^{12}C(^{18}O,^{14}Cα)^{12}C [29]		^{12}C(^{18}O,^{14}Cα)^{12}C [26]	
E_x (MeV)	J $^\pi$	$\Gamma_{\rm tot}$(keV)	BR	θ_α^2	E_x (MeV)	J $^\pi$	$\Gamma_{\rm tot}$(keV)	Γ_α(keV)	θ_α^2	E_x (MeV)	J $^\pi$	E_x (MeV)	J $^\pi$	E_x (MeV)	J $^\pi$
7.11(3)[a]														7.10	4^+
7.62(3)[a]														7.60	1^-
7.86(3)[a]										7.86				7.83	5^-
[8.12(3)][a]										8.04				8.03	1^-
[8.22(3)][a]										8.22				8.21	2^+
8.57(4)[a]															
8.70(4)[a]															
9.06(4)[a]					8.96(1)	(4^+)	70(30)	5(1)	0.20	8.93				8.94	
9.27(4)[a]					9.35(2)	3^-	180(30)	110(30)	0.48	9.35	$(2^+,3^-)$			9.33	
9.63(4)[a]					9.70(1)	3^-	140(10)	15(2)	0.04	9.70	$(1^-,2^+,3^-)$			9.65	
10.28(4)[b]	4^+	39(19)	>0.37(0.03)	0.07	10.290(4)	4^+	29(4)	19(2)	0.09	10.29	$(3^-,4^+,5^-)$	10.29		10.30	4^+
11.13(5)[b]		2(1)	>0.65(0.03)	<0.01 (if 2^+)[d]	10.98(4)	2^+	280(130)	20(10)	0.01						
11.47(5)[b]		61(14)	>0.23(0.01)	0.02 (if 4^+)[d]	11.43(1)	4^+	40(10)	30(10)	0.05					11.39	
				0.07 (if 5^-)											
11.72(5)[b]		32(5)	>0.89(0.03)	0.56 (if 6^+)[d,h]	11.699(5)	6^+	23(2)	12(1)	0.23	11.62	5^-	11.63		11.59	$(5^-,6^+)$
12.38(5)[b]		23(12)	>0.41(0.02)	0.02 (if 5^-)[d,e]	12.339(4)	5^-	39(4)	26(2)	0.06						
12.58(5)[b]		25(8)	>0.79(0.03)	0.02 (if 4^+)[g,h]	12.542(4)	4^+	6(3)	5(2)	<0.01	12.54		12.61	$(2,4,6)^+$	12.55	$(4^+,6^+)$
				0.15 (if 6^+)[d,g,h]	12.576(9)	6^+	70(20)	50(10)	0.38						
12.94(5)[b]		337(16)	>0.94(0.04)	0.10 (if 2^+)[d,f,g]	12.90(3)	2^+	310(30)	285(30)	0.09	13.00	$(2,4)^+$	13.11	$(2,4)^+$		
				0.50 (if 5^-)[d]	12.94(1)	5^-	40(10)	15(2)	0.02						
				0.14 (if 3^-)[d]	12.98(4)	3^-	1040(200)	770(120)	0.32						
13.64(6)[b]		35(26)	>0.07(0.01)	<0.01 (if 2^+)[d]	13.69(1)	2^+	530(120)	40(20)	0.01						
13.87(6)[b]		71(17)	>0.32(0.02)	0.02 (if 5^-)[d]	13.82(1)	5^-	25(6)	3(1)	<0.01			13.94		13.71	
				0.01 (if 4^+)[d]	13.89(1)	4^+	24(10)	14(6)	0.01						
				<0.01 (if 3^-)[d]	13.96(2)	3^-	150(50)	80(10)	0.03						
14.18(6)[b]		169(27)	>0.16(0.01)	0.02 (if 5^-)[d]	14.1(1)	5^-	560(70)	260(20)	0.23						
14.69(6)[b]		21(18)	>0.08(0.01)	<0.01 (if 5^-)[d]	14.7(1)	5^-	280(100)	230(80)	0.16	14.58					
15.88(6)[b]		44(10)	>0.57(0.02)												
16.06(6)[b]															
16.20(6)[b]												16.20			
17.12(6)[b]															
17.42(7)[b]												17.40			
17.81(9)[c]															
18.25(9)[c]															

[a] from events with ^{14}C + $\alpha_{\rm decay}$ detected in the same telescope (L0/R0).
[b] from events with $\alpha_{\rm decay}$ + $\alpha_{\rm recoil}$ detected in two telescopes (L0+R0).
[c] from events with ^{14}C + $\alpha_{\rm decay}$ detected in two telescopes (L0+R0).
[d] possible spin assignment from Ref. [24]
[e] possible spin assignment from Ref. [25]
[f] possible spin assignment from Ref. [28]
[g] possible spin assignment from Ref. [29]
[h] possible spin assignment from Ref. [26]

by the present observation. Thanks to the better energy resolution of the present measurement, as demonstrated above, two peaks can be resolved around 11.6 MeV, with one centroid at about 11.47 MeV and another at about 11.72 MeV (Fig. 5 and Table I). The overlap of these doublets into one state might have led to previous controversial assignments. Now we can reasonably accept 5^- and 6^+ for states at 11.47 and 11.72 MeV, respectively. Then the deduced dimensionless reduced α-width is larger than 0.56 (as shown in Table I). This dominantly large SF for the 6^+ state is strong support for the existence of the positive-parity rotational band with ^{14}C + α molecular structure in ^{18}O. As indicated in Refs. [19, 24], there does exist some fragmentation of the cluster strength for the 4^+ and 6^+ states, but the dominance is still clear in the relevant excitation-energy region. This situation is different from the speculation of Ref. [24].

B. Discussion on the negative-parity band

The α-decay measurement together with the angular correlation analysis by Rae and Bhowmik [26] has given rise to a spin-parity of 1^- to the state at 8.03 MeV in ^{18}O. Later on, possible assignments of $1^-, 2^+$, and 3^- were given to the 9.70-MeV state [28]. Based on some systematics analysis of the inclusive measurement data, combined with theoretical predictions, von Oertzen *et al.* [20] have proposed the $K^\pi = 0_2^-$ negative-parity band with 1^-, 3^-, 5^-, and 7^- members at 8.03, 9.71, 13.62, and 18.63 MeV, respectively. However, measurements by that time were not able to give the α-decay BRs, and therefore, the related cluster-structure probabilities (SFs). Recently, Avila *et al.* [24], based on the resonant scattering experiment and the R-matrix analysis, have extracted very small dimensionless reduced α-widths for the proposed 1^- and 3^- states, and have questioned the existence of this negative-parity band. In the meantime they found several 5^- states with substantial α strength, which spread over 12 to 15 MeV [24]. In the present work, as exhibited in Figs. 5, 6, and 7 and listed in Table I, several strong α-decay states above 12 MeV are observed with much better visibility in comparison to previous α-decay measurements. Among them the states at 12.38, 12.94, 13.87, 14.18, and 14.69 MeV might be of 5^- spin-parity with substantial α strength, according to the R-matrix analysis presented in Ref. [24]. If we adopt this kind of splitting of the 5^- states, the corresponding cluster SFs can be deduced as listed in Table I. However, among these states, most cluster SFs are small, except the one at 12.94 MeV. Again the particular situation is quite different from what is reported in Ref. [24]. It is evident that much more investigation is needed to clarify the existence of the negative-parity band in ^{18}O [19, 24].

V. SUMMARY

A multinucleon transfer reaction ^{9}Be(^{13}C,^{18}O*)α is used to populate the high-lying excited states in ^{18}O. The ^{18}O* $\rightarrow^{14}$C + α decay products and the recoil α-particles were measured by six sets of silicon-strip detectors. ^{14}C + α resonant states were reconstructed from various combinations of detected fragment pairs. The best energy resolution was achieved by using the detected 2-α and deduced ^{14}C events. Exited states in ^{18}O from 7 to 19 MeV were obtained with high resolution and efficiency, owing to the excellent performances of the detectors and their relatively large angular coverage. A number of distinct resonances above 12 MeV were clearly observed, with much better visibility as compared to previously reported results, including several states above 15 MeV observed for the first time.

Using both the missing-mass and the invariant-mass measurements, together with the realistic Monte Carlo simulation for efficiencies, the α-decay branching ratios and the total widths of 14 resonances were extracted. These new direct experimental data were used to deduce the cluster-formation probability (SF) inside the resonant state of ^{18}O. Based on the existing theoretical and experimental investigations, including the presently determined large dimensionless reduced α-width for the 11.7-MeV (6^+) state, the positive-parity band for the ^{14}C + α molecular structure in ^{18}O has been confirmed. On the contrary, the situation for the predicted negative-parity band is quite different. The properties of the primary band members have not be confirmed. It is clear that more exclusive measurements to determine the spins and SFs of the molecular states are badly needed, together with theoretical investigation with more advanced models, to clarify the persistence of the parity-reversion doublet bands and the reflection symmetry in neutron-excess nuclei.

VI. ACKNOWLEDGEMENT

The authors thank the staff of the HI-13 Tandem Accelerator Laboratory at the China Institute of Atomic Energy (CIAE) for their excellent work in providing the beams. This work was supported by the National Key R&D Program of China (Grant No. 2018YFA0404403) and the National Natural Science Foundation of China (Grants No. 11535004, No. 11875074, No. 11775004, No. 11775013, No. 11775316, and No. 11635015).

[1] W. von Oertzen, M. Freer, and Y. Kanada-Enyo, Phys. Rep. **432**, 43 (2006).

[2] H. Horiuchi, K. Ikeda, and K. Kat, Prog. Theor. Phys. Suppl. **192**, 1 (2012).

[3] M. Freer, H. Horiuchi, Y. Kanada-En'yo, D. Lee, and U. Meissner, Rev. Mod. Phys. **90**, 035004 (2018).
[4] H. Horiuchi, K. Ikeda, and N. Takigawa, Prog. Theor. Phys. Suppl. **E68**, 464 (1968).
[5] M. Freer, J. C. Angélique, L. Axelsson, B. Benoit, U. Bergmann, W. N. Catford, S. P. G. Chappell, N. M. Clarke, N. Curtis, *et al.*, Phys. Rev. Lett. **82**, 1383 (1999).
[6] M. Freer *et al.*, Phys. Rev. Lett. **96**, 042501 (2006).
[7] R. J. Charity, S. A. Komarov, L. G. Sobotka, J. Clifford, D. Bazin, A. Gade, L. Jenny, S. M. Lukyanov, W. G. Lynch, *et al.*, Phys. Rev. C **76**, 064313 (2007).
[8] Z. H. Yang, Y. L. Ye, Z. H. Li, J. L. Lou, J. S. Wang, D. X. Jiang, Y. C. Ge, Q. T. Li, H. Hua, X. Q. Li, *et al.*, Phys. Rev. Lett. **112**, 162501 (2014).
[9] Z. H. Yang, Y. L. Ye, Z. H. Li, J. L. Lou, J. S. Wang, D. X. Jiang, Y. C. Ge, Q. T. Li, H. Hua, X. Q. Li, *et al.*, Phys. Rev. C **91**, 024304 (2015).
[10] Z. Yang, Y. Ye, Z. Li, J. Lou, *et al.*, Sci. China: Phys., Mech. Astron. **57**, 1613 (2014).
[11] M. Lyu, Z. Ren, B. Zhou, Y. Funaki, H. Horiuchi, G. Röpke, P. Schuck, A. Tohsaki, C. Xu, and T. Yamada, Phys. Rev. C **93**, 054308 (2016).
[12] W. Jiang, Y. Ye, Z. Li, C. Lin, Q. Li, Y. Ge, J. Lou, D. Jiang, *et al.*, Sci. China: Phys., Mech. Astron. **60**, 062011 (2017).
[13] M. Freer, J. D. Malcolm, N. L. Achouri, N. I. Ashwood, D. W. Bardayan, S. M. Brown, W. N. Catford, K. A. Chipps, J. Cizewski, *et al.*, Phys. Rev. C **90**, 054324 (2014).
[14] J. Li, Y. L. Ye, Z. H. Li, C. J. Lin, Q. T. Li, Y. C. Ge, J. L. Lou, Z. Y. Tian, W. Jiang, *et al.*, Phys. Rev. C **95**, 021303(R) (2017).
[15] H. Yamaguchi, D. Kahl, S. Hayakawa, *et al.*, Phys. Lett. B **766**, 11 (2017).
[16] J. Feng, Y. Ye, B. Yang, C. Lin, H. Jia, D. Pang, Z. Li, J. Lou, Q. Li, X. Yang, *et al.*, Sci. China: Phys., Mech. Astron. **62**, 12011 (2019).
[17] H. L. Zang, Y. L. Ye, Z. H. Li, J. S. Wang, J. L. Lou, Q. T. Li, Y. C. Ge, X. F. Yang, *et al.*, Chin. Phys. C **42**, 074003 (2018).
[18] P. Descouvemont and D. Baye, Phys. Rev. C **31**, 2274 (1985).
[19] N. Furutachi, M. Kimura, A. Dot, Y. Kanada-En'yo, and S. Oryu, Prog. Theor. Phys. **119**, 403 (2008).
[20] W. von Oertzen, T. Dorsch, H. G. Bohlen, R. Krcken, *et al.*, Eur. Phys. J. A **43**, 17 (2010).
[21] H. Horiuchi and K. Ikeda, Prog. Theor. Phys. **40**, 277 (1968).
[22] W. Bauhoff, H. Schultheis, and R. Schultheis, Phys. Rev. C **29**, 1046 (1984).
[23] M. Kimura, Phys. Rev. C **69**, 044319 (2004).
[24] M. L. Avila, G. V. Rogachev, V. Z. Goldberg, E. D. Johnson, K. W. Kemper, Y. M. Tchuvil'sky, and A. S. Volya, Phys. Rev. C **90**, 024327 (2014).
[25] D. Tilley, H. Weller, C. Cheves, and R. Chasteler, Nucl. Phys. A **595**, 1 (1995).
[26] W. Rae and R. Bhowmik, Nucl. Phys. A **420**, 320 (1984).
[27] M. Freer, Nucl. Instrum Methods Phys. Res., Sect. A **383**, 463 (1996).
[28] N. Curtis, D. D. Caussyn, C. Chandler, M. W. Cooper, N. R. Fletcher, R. W. Laird, and J. Pavan, Phys. Rev. C **66**, 024315 (2002).
[29] S. Yildiz, M. Freer, N. Soić, S. Ahmed, N. I. Ashwood, N. M. Clarke, N. Curtis, *et al.*, Phys. Rev. C **73**, 034601 (2006).
[30] N. I. Ashwood *et al.*, J. Phys. G: Nucl. Part. Phys. **32**, 463 (2006).
[31] N. Curtis, D. D. Caussyn, N. R. Fletcher, F. Maréchal, N. Fay, and D. Robson, Phys. Rev. C **64**, 044604 (2001).
[32] W. Rae and R. Bhowmik, Nucl. Phys. A **427**, 142 (1984).
[33] Kisel, Pavel, Kisel, Ivan, Senger, Peter, Vassiliev, Iouri, and Zyzak, Maksym, EPJ Web Conf. **173**, 04009 (2018).
[34] D. L. Price, M. Freer, N. I. Ashwood, N. M. Clarke, N. Curtis, *et al.*, Phys. Rev. C **75**, 014305 (2007).
[35] D. Dell'Aquila, I. Lombardo, L. Acosta, R. Andolina, L. Auditore, G. Cardella, M. B. Chatterjiee, E. De Filippo, L. Francalanza, *et al.*, Phys. Rev. C **93**, 024611 (2016).
[36] A. Cunsolo, A. Foti, G. Imm, G. Pappalardo, G. Raciti, and N. Saunier, Phys. Lett. B **112**, 121 (1982).